is about 10% of the amplitude of the pulse. For narrower pulses, the error is proportional to the square of the pulse width.

This concept is analyzed in Fig 14.5-6. Diagram a is an ideal square input pulse of unit amplitude and pulse width T_p. Diagram b is the integral of this, which is approximated as a step, so that the cross-hatched areas are equal. Each of these areas is equal to $T_p^2/8$. Diagram c is the second integral of the input. The step approximation of the first integral of the input is equivalent to a straight-line approximation of the second integral. The maximum deviation for the second integral is equal to one of the equal cross-hatched areas of diagram b, and so is

$$\mathrm{Max}|D^{-2}x_i| = T_p^2/8 \qquad (14.5\text{-}13)$$

It is convenient to normalize this as follows in terms of the rise time T_R of the step response:

$$\mathrm{Max}|D^{-2}x_i| = \tfrac{1}{8}T_R^2(T_p/T_R)^2 \qquad (14.5\text{-}14)$$

By Eq 14.4-53, the error bound for the approximation is

$$|\mathrm{error}| \le \tfrac{1}{2}(r_{-2} + |a_2|)\mathrm{Max}|D^{-2}x_i|$$
$$\le \tfrac{1}{16}(r_{-2} + |a_2|)T_R^2(T_p/T_R)^2 \qquad (14.5\text{-}15)$$

For the example of Section 14.3, the rise time T_R is 0.01155 sec. As shown in Eq 14.3-26 and Table 14.4-1, for the doublet response the initial-value coefficient a_2 is 1.885×10^4 sec^{-2}, and the remainder coefficient r_{-2} is 3.10×10^4 sec^{-2}. Hence the error bound of Eq 14.5-15 is equal to

$$|\mathrm{error}| \le \tfrac{1}{16}(3.10 + 1.85)(10^4\ \mathrm{sec}^{-2})(0.01155\ \mathrm{sec})^2\left(\frac{T_p}{T_R}\right)^2$$
$$\le 0.413(T_p/T_R)^2 \qquad (14.5\text{-}16)$$

If $T_p = T_R/2$, the error bound is 0.10. Thus, if the pulse width T_p is less than $\frac{1}{2}$ of the step-response rise time T_R, the error associated with approximating the pulse with an impulse is no greater than 10% of the pulse amplitude.

From: Biernson, "Principles of Feedback Control", Vol. 2, Wiley, 1988.

Chapter 15

A Servo for Integrated-Circuit Photolithography

This chapter describes a unique control system that was developed by the author. This was the basis for the GCA wafer-stepping photolithography equipment for fabricating integrated circuits, which exposes the image directly on the silicon wafer. The control system positions an optical stage to a precision of $\frac{1}{15}$ of a wavelength of light over a 6-in. travel. This servo (along with the wafer-stepping approach) provided greatly improved registration accuracy, which allowed the line widths of integrated circuits to be reduced from 5 μm (micrometres, microns) to less than 1 μm. This equipment has resulted in a tremendous increase in the density of integrated circuitry since 1977.

15.1 THE GCA PHOTOREPEATER® FOR WAFER-STEPPING FABRICATION OF INTEGRATED CIRCUITS

This chapter describes the servo system of a step-and-repeat camera (Photorepeater®*) for fabricating integrated circuits, which the author designed in 1974–1976 while working at GCA Corporation. The servo system positions an optical stage in two dimensions to a precision of ±0.040 μm, which is about $\frac{1}{15}$ of a wavelength of visible light. This control system has had a revolutionary effect on integrated circuitry. It was a key element in the development of wafer-stepping photolithography equipment, which allowed the line widths of integrated circuits to be reduced from about 5 μm to less than 1 μm, thereby increasing the circuit density by more than 25:1. (The author was not involved directly in the development of the wafer-stepping process itself, which occurred after he left GCA.)

Step-and-repeat cameras for making integrated circuits built prior to 1976 generally operate in the following manner. A photographic mask, containing

*"Photorepeater" is a registered trademark of GCA Corporation.

the image of one or more integrated circuits for one processing stage, is projected onto a photographic glass plate, typically with a reduction of 10 : 1. The plate is mounted on a photographic stage, which is accurately stepped, one field at a time, so that the image is repeated many times across the plate. After the photographic emulsion on the plate is exposed and developed, the plate is accurately registered on a silicon wafer, and its image is contact-printed onto the wafer. This procedure is repeated with several masks to perform the various stages of the photolithography process. When the processing is completed, the wafer is cut into pieces to make the individual integrated circuits.

The contact-printing process eventually wears the image on the glass plate, and the plate must be replaced. Nevertheless, one glass plate can expose a large number of wafers.

The extremely high precision of the photographic-stage control system designed by the author allowed a new approach to photolithography: the wafer-stepping process. In this process, the image is projected directly onto the silicon wafer, instead of onto a glass plate. Fiduciary marks or details on the first image are sensed optically and used to align subsequent images. The stage is precisely positioned so that each image is accurately registered with the earlier images. Since image registration is performed locally, rather than across the whole wafer, much more accurate registration can be achieved. The increase in registration accuracy has allowed line widths of circuitry elements to be reduced from about 5 μm to less than 1 μm.

The wafer-stepping process resulted in a tremendous increase in the demand for the new GCA step-and-repeat cameras, because the process requires one of these instruments for each assembly station. With the earlier process, one step-and-repeat camera can serve about 50 assembly stations.

A description of this control system is useful, not only because of the practical importance of the process itself, but also because the same control principles can be applied to other systems where ultrahigh positional accuracy is required. One of the requirements for achieving ultrahigh positional accuracy is an ultra-accurate sensor for measuring position and velocity. This was provided by the Hewlett-Packard 5501A laser interferometer, which is discussed in Section 15.2. The stage-control system for this GCA step-and-repeat camera is described in Section 15.3.

15.2 THE HEWLETT-PACKARD 5501A LASER INTERFEROMETER

The Hewlett-Packard 5501A laser interferometer [15.1] is based on a principle called the Zeeman effect. A laser generates two optical waves, which are linearly cross-polarized relative to one another, and which are separated in frequency by about 1.8 MHz. Very accurate distance measurements can be achieved by comparing these optical waves.

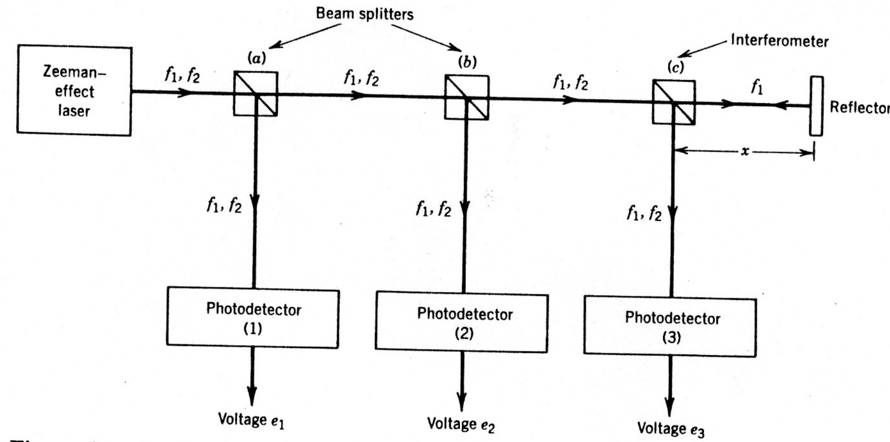

Figure 15.2-1 System showing principle of laser interferometer for measuring position.

A helium–neon laser is used with an output optical power of 1 mW (milliwatt). It operates at a wavelength λ and frequency f of

$$\lambda = 0.632\,999\,37\,\mu\text{m} \tag{15.2-1}$$

$$f = \frac{c}{\lambda} = \frac{2.997\,925 \times 10^8 \text{ m/sec}}{0.632\,999\,37 \times 10^{-6} \text{ m}}$$

$$= 4.73606 \times 10^{14} \text{ Hz} = 4.73606 \times 10^8 \text{ MHz} \tag{15.2-2}$$

The laser light is visible, and has a red color. The optical frequency f is 2.6×10^8 times greater than the 1.8-MHz frequency difference between the two cross-polarized waves.

Figure 15.2-1 illustrates the use of this laser for interferometer distance measurement. The laser transmits two optical frequencies f_1, f_2. Part of this beam is diverted by a beam splitter (a) to a photodetector (1). The output voltage from the photodetector (1) is proportional to the power in the optical wave, and so is proportional to the square of the optical signal. If filtering action is neglected, the signal e_1 from the photodetector (1) is ideally expressed as

$$\text{Ideal}[e_1] = (\cos[\omega_1 t] + \cos[\omega_2 t])^2 \tag{15.2-3}$$

The parameters ω_1, ω_2 are equal to $2\pi f_1, 2\pi f_2$ respectively, where f_1, f_2 are the two optical frequencies separated by 1.8 MHz. Calculating the square in Eq

15.2-3 gives

$$\begin{aligned}\text{Ideal}[e_1] &= \cos^2[\omega_1 t] + \cos^2[\omega_2 t] + 2\cos[\omega_1 t]\cos[\omega_2 t] \\ &= \frac{1+\cos[2\omega_1 t]}{2} + \frac{1+\cos[2\omega_2 t]}{2} \\ &\quad + \cos[(\omega_1+\omega_2)t] + \cos[(\omega_1-\omega_2)t] \qquad (15.2\text{-}4)\end{aligned}$$

The double-optical-frequency components at the frequencies $2\omega_1$, $2\omega_2$, and $(\omega_1 + \omega_2)$ are at such high frequency they are eliminated in the detection process. Hence, the actual photodetector signal reduces to

$$e_1 = 1 + \cos[(\omega_1 - \omega_2)t] \qquad (15.2\text{-}5)$$

The first term is a constant DC term, which is used to measure the signal strength. The interferometer position measurement is derived from the second, AC term, which has a frequency of 1.8 MHz:

$$e_{1(\mathrm{AC})} = \cos[(\omega_1 - \omega_2)t] \qquad (15.2\text{-}6)$$

In Fig 15.2-1, the laser beam is intercepted by a second beam splitter (b), and part of the beam is fed to a second photodetector (2). The optical waves at the surface of the photodetector can be expressed as $\cos[\omega_1 t - \Psi_1]$ and $\cos[\omega_2 t - \Psi_2]$, where the phase shifts Ψ_1, Ψ_2 are equal to

$$\Psi_1 = 2\pi\frac{y}{\lambda_1} \qquad (15.2\text{-}7)$$

$$\Psi_2 = 2\pi\frac{y}{\lambda_2} \qquad (15.2\text{-}8)$$

The parameter y is the additional optical path length to the second photodetector, relative to the first photodetector. Since the wavelengths λ_1, λ_2 for the two frequencies are essentially equal (to within one part in 2.6×10^8), the phase shifts Ψ_1, Ψ_2 are essentially equal. Therefore, the AC signal at the output of photodetector (2) is

$$e_{2(\mathrm{AC})} = \cos[(\omega_1 - \omega_2)t - (\Psi_1 - \Psi_2)] = \cos[(\omega_1 - \omega_2)t] \quad (15.2\text{-}9)$$

This is the same as that in Eq 15.2-6. Thus, the AC signal at the output of a photodetector is independent of the optical path length from the laser.

The laser beam is fed to a third optical element (c), called an interferometer. This device uses the polarization difference between the two waves to separate the f_1-wave from the f_2-wave, and feeds the f_1-wave along an additional path x to the reflector. It is reflected back to the interferometer

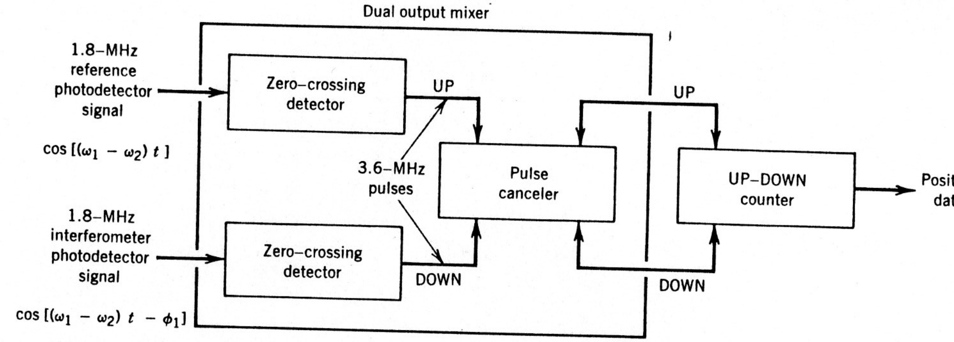

Figure 15.2-2 Block diagram of basic circuitry for decoding interferometer position data.

and combined with the f_2-wave. The combined f_1, f_2 waves are fed to the photodetector (3). The AC output signal from detector (3) is

$$e_{3(\mathrm{AC})} = \cos[(\omega_2 - \omega_1)t - \phi_1] \qquad (15.2\text{-}10)$$

where ϕ_1 is the additional phase shift given to the f_1-signal, which is equal to

$$\phi_1 = \frac{2\pi}{\lambda}2x \qquad (15.2\text{-}11)$$

The variable x is the distance of the reflector from the interferometer. Since the f_1 optical wave travels this distance twice, the variable x is multiplied by 2.

Thus the distance x can be measured by comparing the phase of the 1.8-MHz signal from photodetector (3) at the output of the interferometer with the 1.8-MHz signal from one of the other photodetectors, (1) or (2), which acts as a reference.

Figure 15.2-2 shows how the phase information of the interferometer signal is converted to digital position data. The 1.8-MHz reference and interferometer signals from the photodetectors are fed to zero-crossing detectors, which generate two pulses per cycle of the sinusoid. The resultant 3.6-MHz pulse trains are fed to a pulse-canceler circuit. If there is an excess of UP or DOWN counts, the excess is counted in an UP–DOWN pulse counter. Whenever the phase ϕ_1 of the interferometer signal increases by 180°, an UP pulse is applied to the counter; and whenever ϕ_1 decreases by 180°, a DOWN pulse is applied.

Because of the factor of 2 in Eq 15.2-11, a phase change of 180° occurs whenever x changes by $\frac{1}{4}$ wavelength. It is convenient to consider displacements in microinches. Since one metre is equal to 39.37 inches, one micrometre is equal to 39.37 microinches. Thus, $\frac{1}{4}$ wavelength in micrometres is

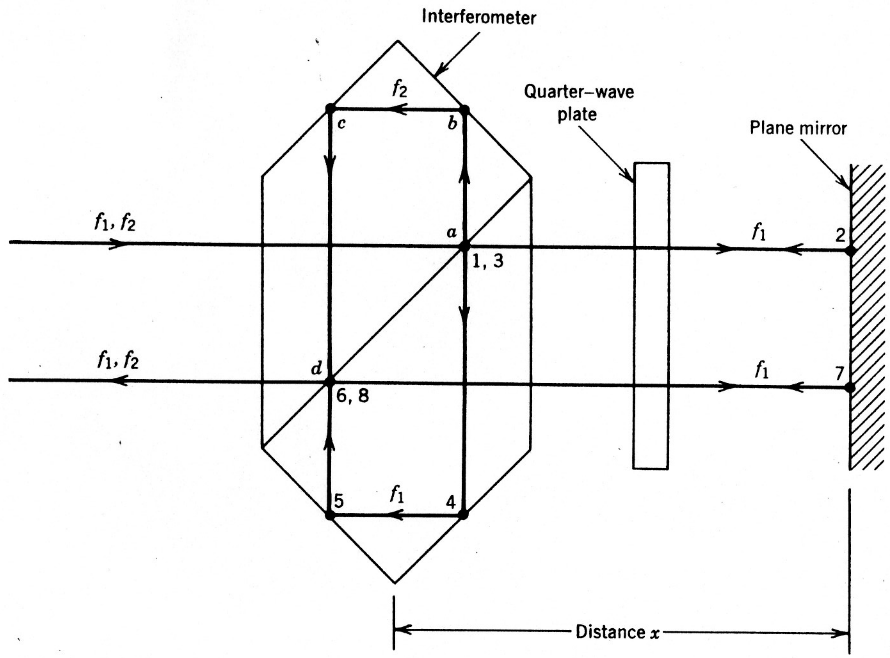

Figure 15.2-3 Paths of laser optical frequencies for plane-mirror interferometer.

(from Eq 15.2-1):

$$\Delta x = \frac{\lambda}{4} = \left(\tfrac{1}{4}\right)(0.6330\ \mu\text{m})(39.37\ \text{in./m}) = 6.2\ \mu\text{in.} \qquad (15.2\text{-}12)$$

Thus an extra pulse is counted for every 6.2-μin. motion of the reflector.

The HP 5501A laser interferometer system may use either a retroflector or a plane-mirror reflector to reflect the f_1 beam. When a plane-mirror reflector is used, a double reflection occurs off the mirror, which doubles the resolution of the interferometer. The resultant optical path is shown in Fig 15.2-3.

In Fig 15.2-3, the reference frequency f_2 travels along path a–b–c–d. Since the f_1 component is cross-polarized, it does not reflect at a. It separates from the f_2 component at point 1, which corresponds to point a, and passes through the quarter-wave plate to point 2 on the mirror. The f_1 component is reflected back through the quarter-wave plate to point 3, at the same location as point 1. The two passes through the quarter-wave plate rotate the polarization of the f_1 component by 90°. Hence the return f_1 component reflects at point 3 along path 3–4–5–6. At point 6 the f_1 component is reflected through the quarter-wave plate to point 7 on the mirror, then back through the quarter-wave plate to point 8. Since the two passes through the quarter-wave plate provide another 90° polarization shift, the reflected f_1 component passes through the mirror and combines with the f_2 component at point 8, which corresponds to point d.

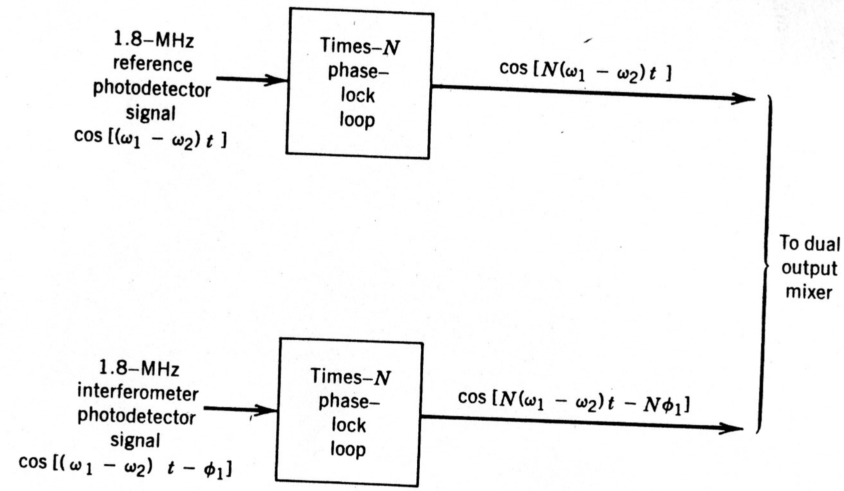

Figure 15.2-4 Block diagram of phase-lock loop circuitry for increasing resolution.

The phase lag imparted to the f_1 component relative to the f_2 component is

$$\phi_1 = \frac{2\pi}{\lambda} 4x \qquad (15.2\text{-}13)$$

where x is the distance of the mirror from the midpoint of the interferometer.

The double reflection off the mirror results in a factor of 4 in Eq 15.2-13. Hence, the basic resolution of the system with the plane-mirror interferometer is $\frac{1}{2}$ of that given in Eq 15.2-12, and so is 3.1 μin. rather than 6.2 μin.

Greater resolution can be achieved by using phase-lock loops in the manner illustrated in Fig 15.2-4. The reference signal and the interferometer signal (which are at 1.8 MHz) are fed to phase-lock loops, which generate phase-coherent frequencies that are N times the input frequency (i.e., sinusoids at 1.8N MHz). This may be achieved by a single phase-lock loop of frequency ratio N, or by cascading loops having a lower frequency ratio. The phase-lock loops increase the phase shift by the factor N. The output signals from the phase-lock loops are fed to the dual output mixer shown in Fig 15.2-2, in place of the photodetector signals. Thus, the resolution is increased by the factor N of the phase-lock loop.

Hewlett-Packard provides phase-lock-loop electronics to extend the resolution by a factor of 16 : 1. Therefore, with a plane-mirror interferometer, the resolution can be decreased by a factor of 16 from 3.1 to 0.2 μin.

15.3 THE SERVO FOR THE GCA STEP-AND-REPEAT CAMERA

15.3.1 Early Step-and-Repeat Cameras

Step-and-repeat cameras that were built in the early 1970s for making integrated circuits typically operate in the following manner. The position of the photographic stage is sensed by linear optical encoders, using analog interpolation to measure a small fraction of an encoder line width. The stage is driven by motor-tachometer servos that are similar to the servo discussed in Chapter 7.

As was shown in Chapter 7, the accuracy of a conventional motor-tachometer servo driving an optical stage is limited by static friction. The example computed a peak static error of 0.2×10^{-3} in. However, this is optimistic, because it ignores the effect of structural dynamics. Probably an accuracy of $\pm 0.5 \times 10^{-3}$ in. is more realistic, which is equivalent to $\pm 12.5\ \mu$m.

This is the accuracy obtainable with conventional positional control. The early step-and-repeat camera achieved much greater accuracy by taking advantage of the principle that friction is nearly constant when the direction of the velocity is constant.

The photographic stage is positioned as follows. The stage is driven to the desired location in a programmed manner. As the desired position is approached, the velocity is decreased linearly. Finally the motor is declutched, and the stage is brought to rest by friction. Since the friction is nearly constant, the stopping trajectory is highly repeatable. The accuracy of positioning is very much better than the $\pm 12.5\ \mu$m achievable by conventional positional control: it is about $\pm 1.0\ \mu$m. Note that this approach cannot allow position corrections to be made after the stage is positioned, a capability that is required in wafer-stepping lithography equipment.

15.3.2 Principles for Eliminating Friction

Much greater positioning accuracy became possible with the availability of the Hewlett-Packard 5501A laser interferometer, described in Section 15.2, which can provide extremely accurate position and velocity data. For a step-and-repeat camera to take advantage of the potential accuracy of this laser interferometer, it must have considerably reduced friction.

There are three basic principles for eliminating friction in a positional control system:

1. Hydraulic bearings.
2. Air bearings.
3. Flexure (spring) mounts.

Hydraulic bearings are not applicable to step-and-repeat cameras, because the hydraulic fluid would contaminate the optical process.

Air bearings have been applied with some success to step-and-repeat cameras. However, an air bearing is inherently a rather soft spring. In order for it to be reasonably stiff, the size of the air-bearing pad must be quite large, and the air gap must be very small—much less than 0.001 in. With such a small air gap, accurate alignment and contamination from dust particles can be serious problems.

The GCA step-and-repeat camera uses the third approach. The fine position stage is supported on flexure (or spring) mounts. The basic principle of flexure mounts is well known. Although the force from a flexure can be quite significant, unlike static friction, this force varies smoothly, and so its effect can be compensated for by an integral network. Hence, a stage mounted on flexures can be positioned to extremely high accuracy.

Because the motion allowable with flexure supports is limited, a two-stage servo is needed when flexures are used. A coarse stage is positioned by conventional means to within about 0.001 in. of the desired location. The coarse stage carries the fine stage, which is mounted on flexures. The fine servo drives the fine stage relative to the coarse stage, to achieve the required ultrahigh accuracy.

15.3.3 Control Configuration of GCA Step-and-Repeat Camera Stage

Figure 15.3-1 shows the control-system configuration of the flexure-mounted photographic stage of the GCA step-and-repeat camera, for a single axis. The position of the coarse stage is controlled by the motor-tachometer servo drive. The fine stage is flexure-mounted onto the coarse stage. The linear actuator (which has no friction) positions the fine stage relative to the coarse stage. The linear variable differential transformer (LVDT) measures the relative displace-

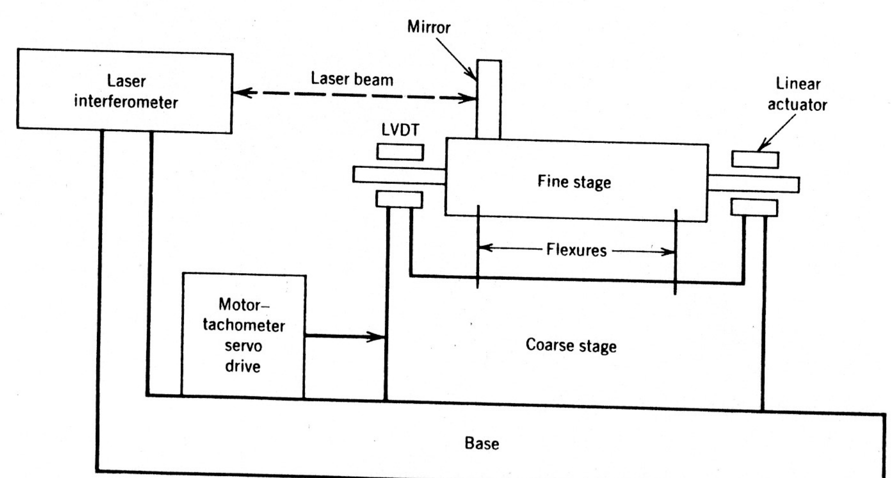

Figure 15.3-1 Basic elements of photographic-stage control system for one axis.

ment between the fine and coarse stage. The laser interferometer measures the absolute position of the fine stage by means of a laser beam, which is reflected off the mirror mounted on the fine stage.

The laser interferometer provides position and velocity data for absolute control of the fine stage. The LVDT measures the relative displacement between the coarse and fine stages. The combination of the laser-interferometer data and the LVDT signal provides position information for control of the coarse stage.

Each axis of the coarse stage is positioned by a tachometer servo, which operates according to the principles discussed in Chapter 7, except that position feedback is derived from a combination of the signals from the laser and the LVDT. When the motor-tachometer drive mechanism positions the coarse stage to approximately the desired position, the motor is declutched, and the coarse stage is brought to rest by friction. Accurate positioning is performed by driving the fine stage relative to the coarse stage by means of the

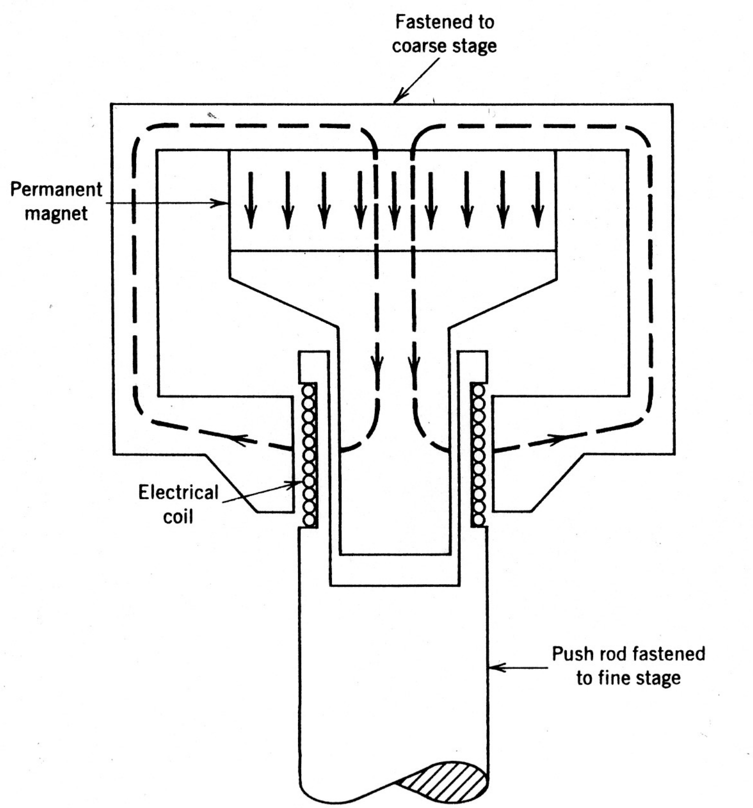

Figure 15.3-2 Principle of frictionless voice-coil-type electromagnet actuator for driving fine stage.

linear actuator. The fine-servo control system derives position and velocity feedback signals from the laser interferometer.

It is essential that the linear actuator and the LVDT have no friction. If appropriately mounted, the LVDT device (which was described in Chapter 8) is frictionless. A frictionless actuator can be achieved by applying the principles of the voice-coil drive in a loudspeaker, in the manner shown in Fig 15.3-2.

The actuator of Fig 15.3-2 consists of a permanent magnet mounted on the coarse stage, and a coil-driven push rod that is coupled to the fine stage. Current flowing through the coil on the push rod applies a force to the fine stage, which is proportional to the coil current.

This actuator mechanism differs from a loudspeaker voice coil in that the push-rod-and-coil mechanism must be very stiff, to provide a high mechanical resonant frequency in the drive. Rather large air gaps can result from the necessary support structure and to allow for motion between the fine and coarse stages. Fortunately, these problems can be counteracted by using a samarium-cobalt permanent magnet, which has an extremely strong magnetic field.

Note that the actuator mechanism that positions the flexure-supported fine stage provides only small motion, whereas an actuator that positions a stage supported on air bearings must provide large motion. It is much more difficult to achieve a frictionless actuator mechanism when the displacement is large.

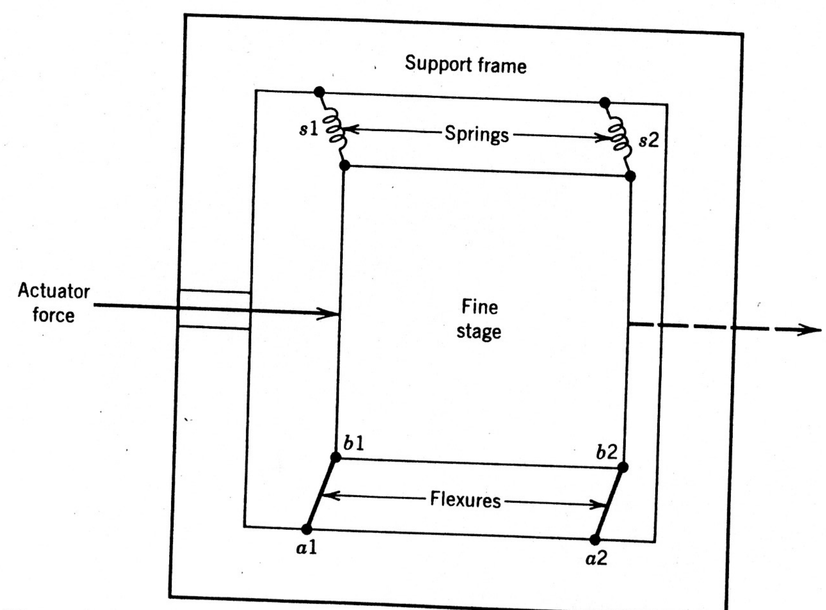

Figure 15.3-3 Basic principle of flexure support of fine stage for motion in a single dimension.

Consequently, the accuracy of a step-and-repeat camera stage supported on air bearings may be degraded by friction in the actuator mechanism.

15.3.4 Flexure Support of Fine Stage

Figure 15.3-3 shows the basic principle for flexure support of the fine stage for motion in a single dimension. The fine stage is supported within the support frame by means of the two flexible supports $a1$–$b1$, $a2$–$b2$, and by the springs $S1$, $S2$. The springs keep the flexible supports in tension. The two flexible supports form a parallelogram ($a1$–$b1$–$b2$–$a2$), which keeps the lines $a1$–$a2$ and $b1$–$b2$ parallel. Thus, the fine stage can only move in a single dimension, without rotation, within the support frame.

Figure 15.3-4 gives a more practical mounting scheme, which is equivalent to that of Fig 15.3-3. The fine stage is supported by two straps $a1$–$b1$–$c1$–$d1$ and $a2$–$b2$–$c2$–$d2$. One end of each strap ($a1$, $a2$) is connected to the support frame, and the other end ($d1$, $d2$) is connected to one of the blocks ($B1$, $B2$). The blocks $B1$, $B2$ are coupled to the frame by means of the strap springs $S1$, $S2$, which keep the support straps $a1$–$b1$–$c1$–$d1$ and $a2$–$b2$–$c2$–$d2$ in tension.

The flexure support mechanism in Fig 15.3-4 keeps the surface of the fine stage in a horizontal plane (parallel to the surface of the paper). The stage is allowed to move (without rotation) only in a single dimension.

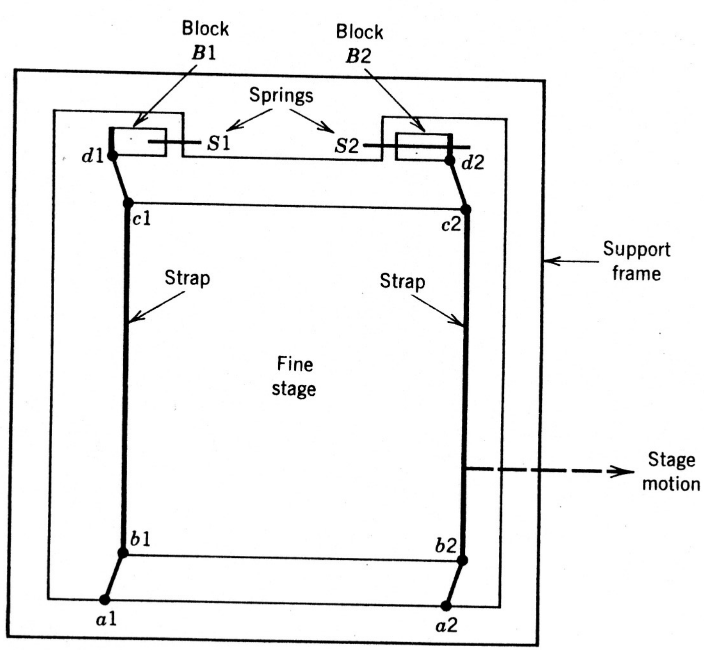

Figure 15.3-4 Practical design of flexure support of fine stage for motion in a single dimension.

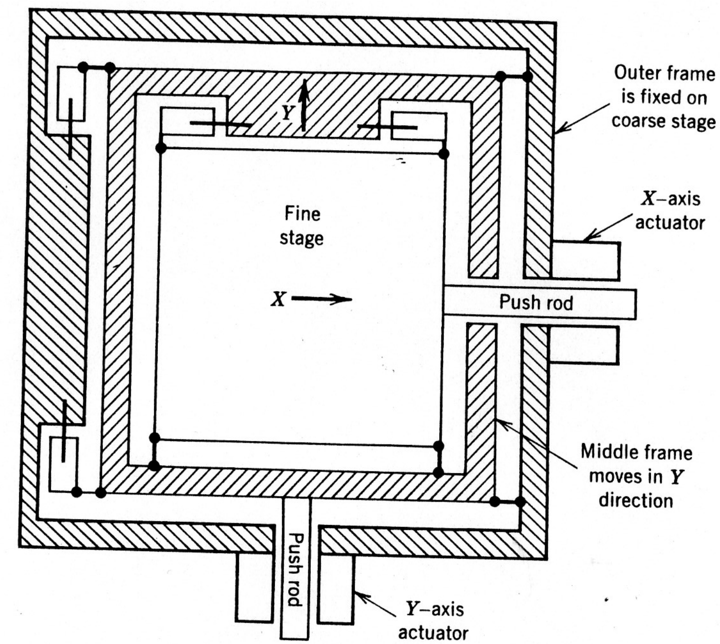

Figure 15.3-5 Two-axis flexure support for fine stage.

Figure 15.3-5 shows the principle of a two-axis flexure mount for supporting the fine stage on the coarse stage. The fine stage is fastened by means of flexures to the middle frame. The flexures allow the fine stage to move relative to the middle frame in the X-direction. The middle frame is fastened by means of flexures to the outer frame (attached to the coarse stage). These flexures allow the middle frame to move in the Y-direction, relative to the coarse stage. The fine stage moves in the Y-direction along with the middle frame. The X and Y actuators drive the fine stage relative to the coarse stage in the X and Y directions.

The two-axis flexure mount illustrated in Fig 15.3-5 shows the well-known principle of supporting an instrument stage by means of flexures, to allow two-axis motion. The actual flexure support used in the GCA step-and-repeat camera applies this principle, but differs in mechanical details.

15.3.5 Summary of Operation of Photographic-Stage Servo

The coarse stage of the GCA step-and-repeat camera is driven in the X and Y directions by tachometer-feedback DC electric servos, which are similar to the servo discussed in Chapter 7. Each servo has a current feedback loop, a tachometer velocity loop, and a position loop. The error signal for the position loop is derived from (1) the digital position command, (2) the digital position feedback signal obtained from the laser interferometer, and (3) the analog signal from the LVDT, which measures the displacement between the fine and coarse stages. These servos drive the coarse stage to approximately the desired position, to an accuracy of the order of 0.001 in. Then the motor is declutched, and the coarse stage is held fixed by friction.

The fine stage is driven in the X and Y directions by means of electromagnetic voice-coil-type actuators. A current feedback loop provides precise control of the actuator current, which is proportional to the force exerted by the actuator on the fine stage.

The position of the fine stage is measured to a precision of 1.5 μin. by the Hewlett-Packard 5501A laser interferometer. A flat-mirror interferometer is used, which has a basic resolution of 3 μin. A phase-lock loop increases this resolution by a factor of 2 : 1, to achieve a final position resolution of 1.5 μin., which is equivalent to 0.040 μm.

Velocity feedback information is achieved by using phase-lock loops to provide laser position data of very fine resolution. These fine laser-interferometer pulses are counted over a fixed time interval to obtain a velocity signal. For example, phase-lock-loop electronics supplied by Hewlett-Packard can provide a 16 : 1 increase in resolution. For a flat-mirror laser interferometer, which has a basic resolution of 3 μin., the resolution with a 16 : 1 phase-lock-loop ratio is 0.2 μin. If these 0.2-μin. pulses are counted over a period of 1 millisecond (msec), the resultant velocity resolution is

$$\Delta V = (0.2\ \mu\text{in})/(1\ \text{msec}) = 2 \times 10^{-4}\ \text{in./sec} \tag{15.3-1}$$

Nominal values for the primary dynamic parameters of the fine position servo are as follows:

Velocity-loop gain crossover frequency:

$$\omega_{cv} = 250\ \text{rad/sec}\ (40\ \text{Hz}) \tag{15.3-2}$$

Position-loop gain crossover frequency:

$$\omega_{cp} = 100\ \text{rad/sec}\ (16\ \text{Hz}) \tag{15.3-3}$$

Break frequency of position-loop integral network:

$$\omega_{ip} = 25\ \text{rad/sec}\ (4\ \text{Hz}) \tag{15.3-4}$$

For the position-loop gain crossover frequency ω_{cp} of Eq 15.3-3, the velocity error ΔV of Eq 15.3-1 would produce the following error in position:

$$X_e = \frac{\Delta V}{\omega_{cp}} = \frac{2 \times 10^{-4}\ \text{in./sec}}{100\ \text{sec}^{-1}} = 2 \times 10^{-6}\ \text{in.} = 2\ \mu\text{in.} \tag{15.3-5}$$

On the other hand, the servo system averages the returns from many velocity samples, and so the resultant position error is appreciably smaller than this.

The resolution achievable from the laser velocity signal is critically dependent on noise in the electronic circuitry that processes the laser-interferometer signal. A strong factor in the extremely fine precision achieved by the GCA equipment was the excellent low-noise design of the phase-lock loops and other circuits for processing the laser signal. This circuitry was designed at GCA by Edward Radziewicz.

In order for this servo system to step quickly, it includes a great many nonlinear controls, which allow the system to switch rapidly from coarse to fine control, with minimum transients. The position of the fine stage relative to the coarse stage is controlled during the coarse step in order to minimize settling time. In tests performed by the author, the system could step 0.1 in. and be within an error of ± 6.2 μin. (± 0.16 μm) in 0.5 sec. The final position was held to a precision of ± 1.5 μin.

15.3.6 A Structural-Resonance Problem Encountered during Development

As in the design of any high-performance servo system, structural dynamics was an important issue. However, a particularly acute structural-resonance problem was experienced in the development of this equipment, which serves as a good illustration of the basic principle: In servo development, structural dynamics should be treated with a great deal of respect.

The first prototype step-and-repeat camera had been constructed, and I started to optimize the feedback loops of the fine X and Y control systems. Dynamic parameters were soon achieved that were reasonably close to the desired values. The next day, I attempted to repeat the tests, and the servo started to oscillate at 40 Hz. I struggled with this problem for several days, but nothing I did could stop this erratic oscillation, which would strangely appear and disappear.

Finally, I received assistance from a well-seasoned engineer, with tremendous engineering insight. After watching me struggle with the problem for a while, Paul Dippolito quietly stated, "George, you have a rotary oscillation mode."

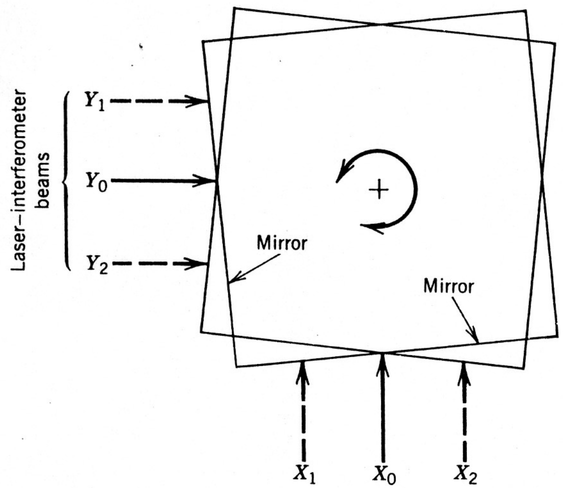

Figure 15.3-6 Rotary oscillation of fine stage.

Once he explained the problem, it was obvious what was happening. The fine stage was oscillating in a rotary fashion about the vertical axis, as shown in Fig 15.3-6. When the coarse stage was positioned in the center of the 6-in. range of motion, the laser beams would reflect off the mirrors along lines X_0 and Y_0. For these beam positions, the rotary oscillation did not cause any changes of optical path length, and so did not couple into the X and Y control loops. However, when the coarse stage was positioned off center, the light beams were in locations such as X_1, X_2, Y_1, Y_2. For these locations, the rotation caused a change in the measured distance. The rotary motion would couple into the position and velocity loops, causing the fine servo to oscillate.

Thus, when the tests were performed with the coarse stage near the center of the field, the servos would work. However, when the coarse stage was moved sufficiently off from the center of the field, the rotary mode was excited, and the servo would oscillate.

Several of us began to examine the flexure support of the fine stage to determine the cause of the rotary oscillation. Remember, from the discussion in Section 15.3.4, that the flexures are supposed to keep the fine stage from rotating, and to allow only linear motion in the X and Y directions. However, the collection of straps and blocks in the flexure-support mechanism made the problem seem very complicated.

While I was missing the point, Paul Dippolito again came forth with the answer, along with mechanical measurements he had taken to prove his conclusion. The middle frame in Fig 15.3-5 was distorting from the shape of a rectangle to a parallelogram, because it was weak in bending at its corners. This distortion of the middle stage allowed the fine stage to rotate. The outer frame could not distort, because it was mounted firmly onto the coarse stage.

Tests were performed on this rotary oscillation mode by recording the decay of the oscillation after the excitation was removed. The oscillation decayed by 1.8% from one cycle to the next, which indicated that the logarithmic decrement δ was 1.8%. In accordance with the equations in Chapter 10, Section 10.4.2, the corresponding value of resonance amplification factor Q was 170, and the damping ratio ζ was 0.003.

This rotary oscillation mode, with its extremely high Q, was weakly coupled to the control loops of the fine stage. Consequently, the mode could not be observed in an open-loop frequency-response test. However, when the loops were closed, enough energy could couple into this high-Q mode to cause oscillation.

The rotary-oscillation problem was corrected by fastening a plate across the under side of the middle frame. This plate, which passed under the fine stage, greatly increased the stiffness of the middle frame, and so prevented the parallelogram distortion. With this increase in stiffness, the 40-Hz oscillation was eliminated.

As pointed out in the Preface, I became acutely aware of structural resonance in the early 1950s, when performing frequency-response tests on an aircraft fire-control system. Over the years, I had encountered structural-dynamics problems again and again. Yet, here in my tests on this control system, I was floored by the mysterious oscillation. Instinctively, I felt it was due to structural resonance, but the precise cause eluded me.

Difficulties like this can be frustrating. However, the struggle to overcome them is what makes feedback control such an exciting area in which to work.

■ A new 4X, 31.11 mm-diameter, high-NA, double-telecentric lens provides automatic control and optimization of numerical aperture settings, magnification, distortion, and field curvature.

■ A broadband, field-by-field, focusing and leveling system guarantees both optimum critical dimension control and high throughput.

■ ASML is the only stepper manufacturer with a DUV direct-reticle, referenced-through-the-lens, phase-grating alignment system. This improves alignment accuracy and — combined with the high-speed, precision, air-bearing stage — delivers superior overlay performance.

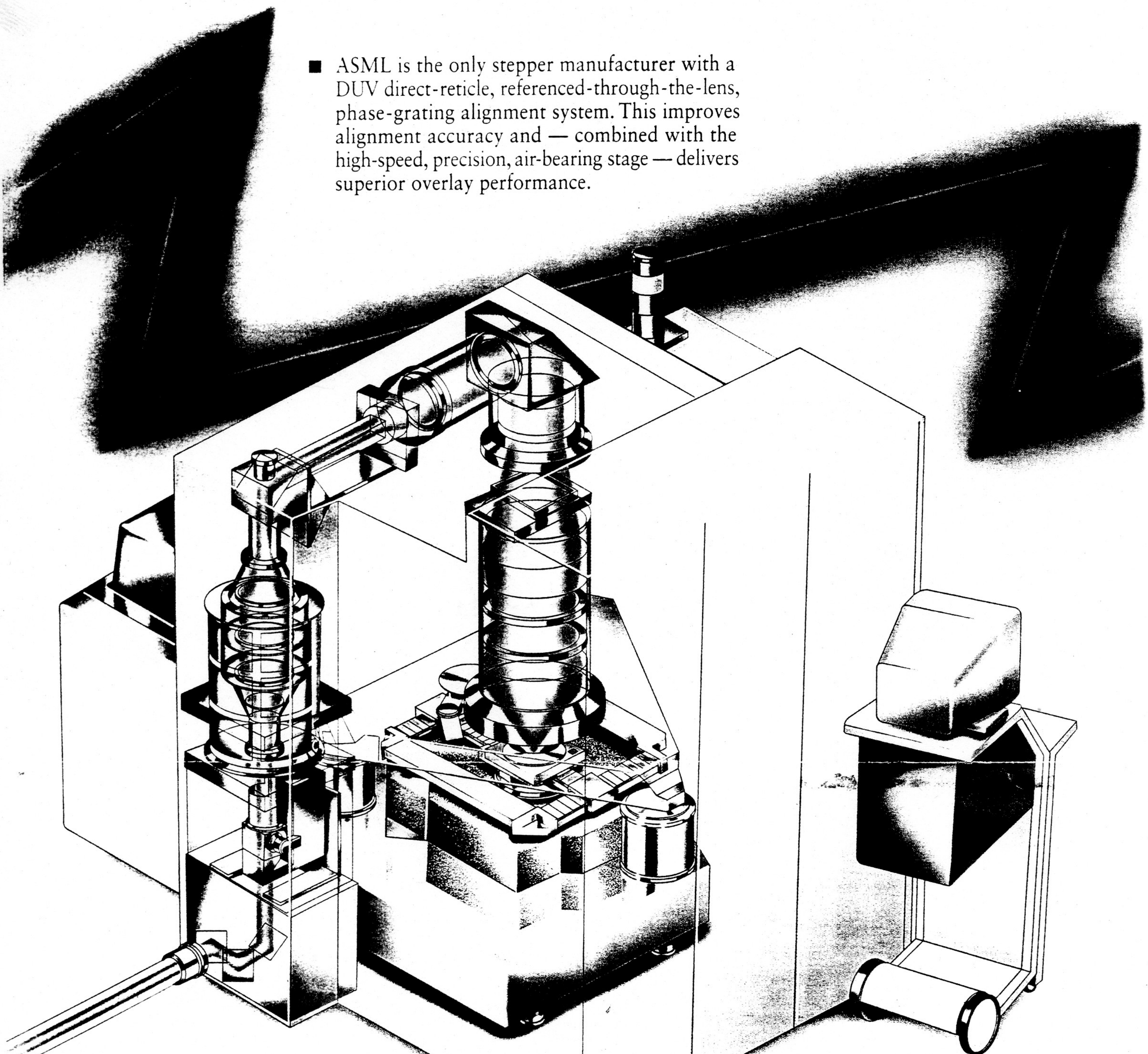

■ The new DUV AERIAL Illuminator automatically enhances resolution, extends process latitude, and delivers industry-leading intensity.

■ Class 1 laminar air flow with optional active charcoal filtration is delivered throughout the stage and wafer-transfer area. This ensures contamination-free operation for consistently high yields in your production environment.